

## Induced-Charge Capacitive Deionization: The Electrokinetic Response of a Porous Particle to an External Electric Field

S. Rubin,<sup>1</sup> M. E. Suss,<sup>1</sup> P. M. Biesheuvel,<sup>2</sup> and M. Bercovici<sup>1,\*</sup>

<sup>1</sup>Faculty of Mechanical Engineering, Technion–Israel Institute of Technology, Haifa 3200003, Israel

<sup>2</sup>Wetsus, European Centre of Excellence for Sustainable Water Technology, Oostergoweg 9, 8911 MA Leeuwarden, The Netherlands

(Received 4 July 2016; revised manuscript received 28 September 2016; published 2 December 2016)

We demonstrate the phenomenon of induced-charge capacitive deionization that occurs around a porous and conducting particle immersed in an electrolyte, under the action of an external electric field. The external electric field induces an electric dipole in the porous particle, leading to its capacitive charging by both cations and anions at opposite poles. This regime is characterized by a long charging time, which results in significant changes in salt concentration in the electrically neutral bulk, on the scale of the particle. We qualitatively demonstrate the effect of advection on the spatiotemporal concentration field, which, through diffusiophoresis, may introduce corrections to the electrophoretic mobility of such particles.

DOI: 10.1103/PhysRevLett.117.234502

**Introduction.**—The study of electrokinetic effects dates back to the 19th century [1,2], and encompasses the interaction between ions, fluid flows, electrical fields, and suspended particles. In the past two decades electrokinetics attracted much interest in the context of microfluidic systems, due to favorable scaling of mass transport with miniaturization, which has led to a wide range of applications in bioanalysis and flow control and also stimulated theoretical investigation of novel physical regimes. The formation of an electric double layer (EDL) at the solid-fluid interface has been a central object of research for more than a century, and yet many aspects of its rich multiscale physics remain to be explored. Surface charge on a solid can be established by its chemical interaction with the liquid, or can be induced by an external electric field (see Ref. [3] and references therein). While the electrokinetic response of a polarizable impermeable particle subject to an external electric field (i.e., the induced-charge mechanism) has been thoroughly investigated both theoretically and experimentally [3–6], to the best of our knowledge the response of a porous polarizable particle has not been addressed to date.

In this Letter we study the response of a conducting porous particle, characterized by a large surface-to-volume ratio, to an externally applied dc electric field. Owing to the large surface area, the polarization of the particle's surface leads to a new physical regime in induced-charge electrokinetics, characterized by a long charging time and non-linear dynamics in the electrically neutral bulk, which generates large depletion regions (on the order of the particle). The charging process can be described by source terms in the porous particle, and when coupled with electromigration, diffusion and advection (e.g., pressure driven, or by induced-charge electroosmosis) results in spatial distributions of salts, which are fundamentally

different from those obtained in capacitive charging of impermeable particles. We experimentally investigate this regime around a fixed particle using a binary electrolyte in which one of the ions is fluorescent and provide a two-dimensional model that qualitatively captures key properties of this process. Our analysis also indicates the importance of such electroosorption on the electrophoresis of polarizable porous particles.

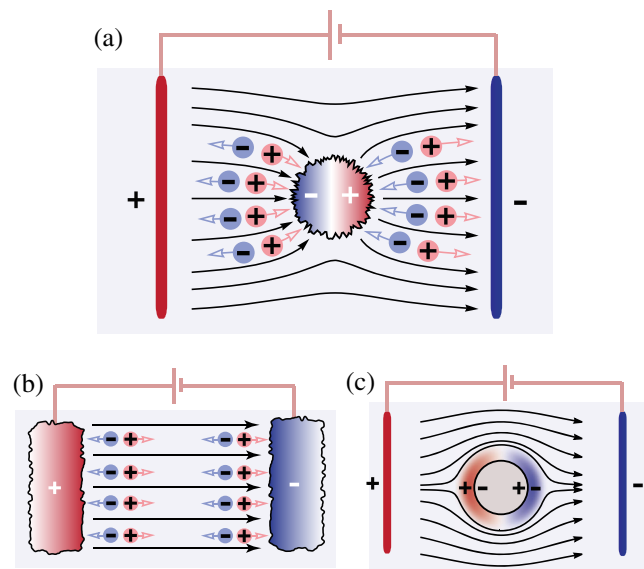


FIG. 1. (a) In ICCDI, an external electric field induces an electric dipole on a porous solid which leads to its capacitive charging over long durations of time. (b) In a typical CDI configuration an electrolyte is deionized by a pair of porous conducting electrodes connected directly to a power source, (c) in contrast to ICCDI the EDL of an impermeable and polarizable particle rapidly charges, resulting in nonpenetrating electric field lines.

The first studies on ion transport within and around porous electrodes [7–10] were initiated in the 1960s. These processes, commonly referred to as capacitive deionization (CDI), are of great interest for their potential applications [11–16], which include water desalination and energy storage. Figure 1 illustratively compares the induced-charge capacitive deionization (ICCDI) regime, which is the subject of our study, with the cases of CDI and of an impermeable induced-charge particle. In standard CDI [Fig. 1(b)], a power source is connected to two separate porous electrodes, such that one acts as a cathode and the other as an anode. The deionization processes occur as negative and positive ions electromigrate towards the anode and cathode, respectively. Similarly, in the ICCDI regime positive and negative ions, from around and inside the porous particle, are electrosorbed (or expelled) at its two oppositely charged regions. Figure 1(c) presents the process of induced charge around an impermeable conducting particle at the low Dukhin number ( $Du$ ) regime [17,18]. In this regime the EDL quickly achieves equilibrium, and changes to ionic concentrations are limited to the EDL. At high surface conductance [ $Du \sim O(1)$  or higher], significant concentration polarization arises, characterized by enrichment regions perpendicular to the applied electric field and by depletion regions parallel to it [5,19], accompanied by penetration of charge into the bulk. In marked difference, the ICCDI regime results in continuous growth of large depletion regions (on the order of the particle's size) in the electrically neutral bulk, which are the result of the particle's large surface-to-volume ratio. Notably, this regime is independent of surface conductance and holds even for  $Du \ll 1$  and moderate electrical fields.

*Theoretical analysis.*—We begin by considering ion transport in porous media with a bimodal pore size distribution, characterized by a hierarchical structure having two types of pores. For activated carbon, relevant for our study, these are electroneutral macropores of a typical scale of  $1 \mu\text{m}$  and electrically charged micropores with overlapping EDLs of a typical scale of  $1 \text{ nm}$ , which occupy regions of porosities  $p_M$  and  $p_m$ , respectively [7,20–25]. In our notation, the subscripts  $m, M, B$  indicate a physical quantity within the distinct regions of the micropores ( $m$ ), macropores ( $M$ ), and bulk ( $B$ ), whereas  $+, -$  distinguish between cations and anions. In the macropores and the bulk, the current density of ionic species in a binary and symmetric electrolyte ( $z = z^\pm > 0$ ), due to diffusion, advection field  $\vec{u}$ , and electromigration, is given by

$$\vec{J}_{M,B}^\pm = -(D_{M,B}^\pm \vec{\nabla} c_{M,B}^\pm \mp Fz b_{M,B}^\pm c_{M,B}^\pm \vec{\nabla} \varphi_{M,B} - c_{M,B}^\pm \vec{u}), \quad (1)$$

where  $F$  is the Faraday constant,  $\varphi$  is the electrostatic potential, and  $b^\pm$  and  $D^\pm$  are, respectively, the effective electrophoretic mobilities (which account for finite dissociation and ionic strength effects) and the diffusion

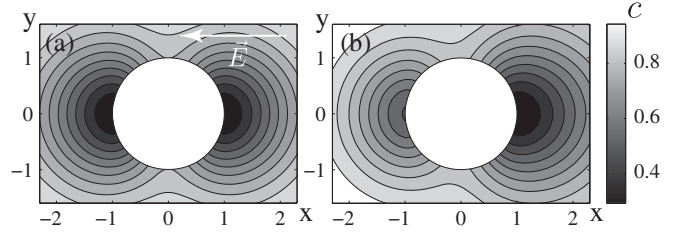


FIG. 2. Numerical simulation results at a nondimensional time  $0.5$  (scaled by  $a^2/D$ ) [26], showing changes in the initial uniform concentration distribution ( $c_0 = 1$ ) due to electrosorption invoked by ICCDI around a porous disk. Panel (a) presents the symmetric case, while panel (b) shows the asymmetric case where the positive ion has a higher mobility than the negative ion, and a larger depletion region forms around the negative pole.

coefficients. In light of better agreement with some experimental regimes [20,22–24], we here adopt the modified Donnan (MD) model for capacitive charging, which assumes no transport in the micropore region, but note that the qualitative results of our study remain unchanged when using the Gouy-Chapman model. The governing Nernst-Planck equations for ionic species in the macropore region take the form

$$\frac{\partial c_M^\pm}{\partial t} + \frac{1}{p_M} \vec{\nabla} \cdot (p_M \vec{J}_M^\pm) = -I_S, \quad (2)$$

where  $I_S$  is a source term representing the consumption of ions in the micropores [20] (see Ref. [26] for an explicit expression). A similar equation with  $p_M = 1$  and  $I_S = 0$  holds in the bulk. The potential difference between the electrode surface and macropore space,  $\varphi_e - \varphi_M$ , is the sum of the Donnan potential ( $\Delta\varphi_D$ ), which represents the total potential drop between the macropores and the micropores, and the Stern potentials ( $\Delta\varphi_S$ ), which represents the potential jump between the micropores and the surface (see Ref. [26] for an explicit expression),

$$\varphi_e - \varphi_M = (\varphi_e - \varphi_m) + (\varphi_m - \varphi_M) = \Delta\varphi_S + \Delta\varphi_D. \quad (3)$$

For convenience, we express Eqs. (1)–(3) as a function of the (half) neutral salt concentration and (half) charge density defined by  $c = (c^+ + c^-)/2$  and  $\rho = Fz(c^+ - c^-)/2$ . The dynamics in the bulk and macropore regions is linked through matching conditions which stem from mass and charge conservation (see discussion in Ref. [26]).

Before turning to numerical solutions of the nonlinear governing equations for ion transport Eqs. (1)–(3), we seek to gain some insight by analyzing the angular distribution of the salt concentration and of the electrostatic potential at early times. To this end, we consider again the case of no advection ( $\vec{u} = 0$ ), consider a symmetric case of equal diffusion coefficients,  $D_{M,B}^+ = D_{M,B}^-$ , and perform Taylor

expansion of salt concentration and electric potential up to second order in time  $\delta t$  via  $c = c_0 + \delta c + \delta^2 c + \dots$  and  $\varphi = \varphi_0 + \delta\varphi + \delta^2\varphi + \dots$ . The corresponding relations that couple  $\delta^2 c$  and  $\delta\varphi$  take the form

$$\nabla^2 \delta\varphi = B \frac{\partial \delta\varphi}{\partial t}, \quad (4a)$$

$$\frac{\partial \delta^2 c}{\partial t} - \nabla^2 \delta^2 c = A \delta\varphi \frac{\partial \delta\varphi}{\partial t}, \quad (4b)$$

and are, in principle, model independent.  $A$  and  $B$  are positive coefficients that can be calculated for both Gouy-Chapman and MD capacitive charging models [26]. Note that the term  $\partial\varphi/\partial t$  can be eliminated by substituting Eq. (4a) into Eq. (4b), resulting in an equation which directly relates the leading term of the potential  $\delta\varphi$  to the leading term of the concentration  $\delta^2 c$ ,  $\partial\delta^2 c/\partial t - \nabla^2 \delta^2 c = A/B \times \delta\varphi \nabla^2 \delta\varphi$ . At short times,  $\delta\varphi$  admits an initial behavior of a dipole, i.e.,  $\cos(\theta)$  dependence, where  $\theta$  is the angle with respect to the horizontal axis, in a coordinate system concentric with the disk. This angular dependence of  $\delta\varphi$  serves as a consistent initial condition for Eq. (4a). Since tangential derivatives in concentration along the edge of the disk are expected to be much smaller than radial ones, the tangential components in the Laplacian of Eq. (4b) can be neglected, indicating that  $\delta^2 c$  must admit an angular dependence of  $\cos^2(\theta)$ . The most significant depletion regions in the electroneutral bulk are thus anticipated at the poles ( $\theta = 0, \pi$ ) of the disk, which also occurs for diffuse charge distribution in the EDL around an impermeable and ideally polarizable disk [29].

To obtain the dynamics over longer times, we turn to a two-dimensional numerical simulation. To this end, we use a finite elements software (COMSOL Multiphysics [30]) to solve the set of Nernst-Planck equations Eq. (2) and the MD model for capacitive charging (see Ref. [26] for detailed information on the simulation). For simplicity, we first focus on the case of  $\vec{u} = \vec{0}$ . Figures 2(a) and 2(b) present numerical solutions of the salt concentration distribution for the cases of a symmetric and a nonsymmetric electrolyte, respectively. Consistent with our analysis for early times, we indeed obtain the most significant depletion in the vicinity of the two poles. Furthermore, for the asymmetric case, characterized by the positive ions having a higher effective electrophoretic mobility than the negative ions, the larger depletion region, presented in Fig. 2(b), forms around the negative pole.

For an impermeable polarizable particle, the charging time  $\tau_{\text{ch}}$  is on the order of the charge relaxation time  $\lambda_D a/D$  (where  $\lambda_D$  is the Debye length scale [31]) and introduces concentration changes on the order of  $\sqrt{\lambda_D/a}$  over a narrow region of  $\sqrt{\lambda_D a}$  [32]. For  $a = 1$  mm,  $\lambda_D = 100$  nm, and  $D = 10^{-9}$  m<sup>2</sup>/s, this corresponds to  $\tau_{\text{ch}} = 100$  ms and a 1% change in concentration over a

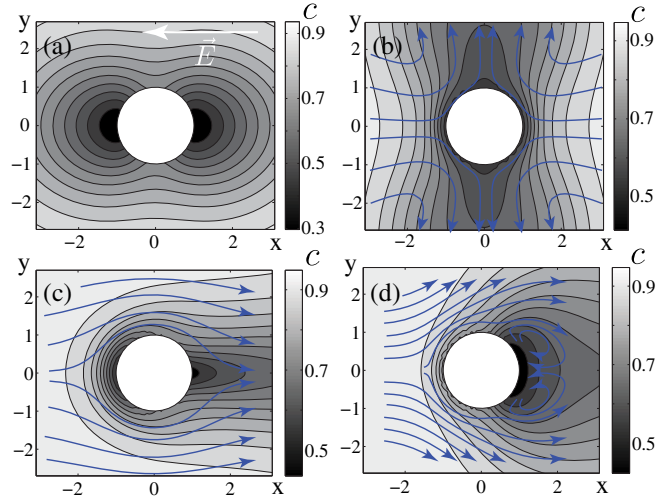


FIG. 3. Numerical simulation results at a nondimensional time 1 (scaled by  $a^2/D$ ) [26], showing the concentration distribution due to the combined effect of ICCDI, uniform flow (either pressure driven or electroosmotic), and ICEO on a porous cylinder. (a) In the absence of advection, depletion regions are formed at  $\theta = 0, \pi$ . (b) With strong ICEO, convection shifts the depletion toward the  $\theta = \pm\pi/2$ . (c) Under uniform flow, the left depletion region diminishes, while the right one is extended. In (b) and (c) the maximum slip velocity is set as  $16D/a$ . (d) Illustration of the combined effect of ICEO and advection.

$10 \mu\text{m}$  region. In contrast, while the charge relaxation time in ICCDI remains unchanged, the actual charging time  $\tau_{\text{ch}}$  depends both on the availability of ions around the porous particle and on their propagation within the porous region. However, for a diffusion limited process  $\tau_{\text{ch}}$  is simply determined by the diffusion time scale in the bulk,  $\tau_D = a^2/D$ . In cases where advection is present the availability of ions increases and charging rate grows. Figure S5 in Ref. [26] shows the flux of salt into the porous disk as a function of time, at different slip velocities, for both dipolar and quadrupolar flows.

Beyond aspects for charging time, advection in the bulk affects the spatial distribution of salt. This is an inherently unsteady process, in which the time-dependent electro-sorption operates at similar rates as diffusion and advection. Figure 3 presents numerical simulation results showing the concentration distribution for ICCDI cases, which also include advection. We show the cases of dipole and quadrupole flows, which correspond, respectively, to the cases of native electro-osmosis and induced-charge electro-osmosis (ICEO) [3].

It is worth noting the relevance of ICCDI to electro-phoresis and diffusiophoresis of mobile porous (and polarizable) particles. In particular, the self-generated salt gradient over the scale of the particle introduces a retardation force due to osmotic pressure in the direction of  $\vec{\nabla}c$  (the so-called chemiophoretic term [33,34]) and an additional electric force that stems from the difference in

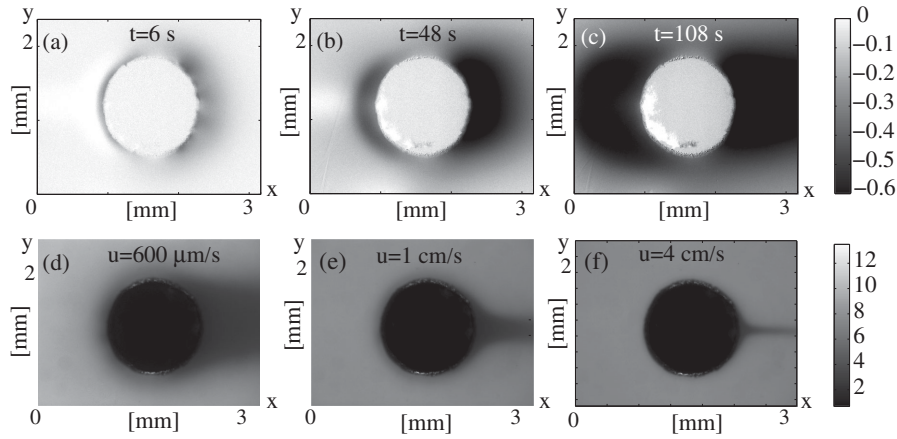


FIG. 4. Experimental results showing the concentration field due to ICCDI. Images show fluorescence signal of  $100 \mu\text{M}$  sodium fluorescein under an applied potential difference of 20 V between the right and left electrodes, around a 1.2 mm diameter carbon disk at times (a) 6 s, (b) 48 s, and (c) 108 s. Each frame (a)–(c) presents the change in fluorescence relative to the first frame, and is normalized by it for flat-field correction. (d)–(f) Raw fluorescence images showing the combined effect of ICCDI with pressure-driven flow from left to right, at different flow velocities  $u$ : (d)  $600 \mu\text{m/s}$ , (e)  $1 \text{ cm/s}$ , (f)  $4 \text{ cm/s}$ .

diffusivities of the cations and the anions. The latter generates an additional electrophoretic term given by  $(3/2z^2)(D^+ - D^-)/(D^+ + D^-)(k_B T/6\pi\eta\lambda_B)(\zeta/V_T) \times \vec{\nabla} \log(c/c_0)$ , which, depending on the sign of  $\zeta(D^+ - D^-)$ , is directed with or against the direction of  $\vec{\nabla} c$  [33,35]. Typical values of  $\zeta = 75 \text{ mV}$ ,  $k_B T/6\pi\eta\lambda_B = 350 \mu\text{m}^2/\text{s}$ ,  $\lambda_B = 0.7 \text{ nm}$ , and  $\Delta c/c = 1/10$  lead to velocities on the order of  $100 \mu\text{m/s}$  for a  $100 \mu\text{m}$  diameter particle. Notably, relatively high electric fields are required in order to activate the nonlinearity which, through surface conduction, results in retardation of an impermeable polarizable particle [18]. In contrast, the asymmetric salt gradient around a porous particle gives rise to nonlinearities even at low fields, and may result in either retardation or advancement.

*Experimental results.*—We experimentally investigated the process of ICCDI by placing a disk-shaped activated porous electrode (1 mm diameter) in an acrylic microfluidic chamber ( $W \times L \times H = 15 \text{ mm} \times 75 \text{ mm} \times 250 \mu\text{m}$ ) containing a binary electrolyte solution of  $100 \mu\text{M}$  sodium fluorescein. We applied an external electric potential difference of 20 V from electrodes situated in two reservoirs located at the far ends of the chamber 75 mm apart (the estimated value of a uniform electric field component  $E_0$  is  $260 \text{ V/m}$ ). This setup is mounted on top of an inverted epifluorescence microscope (see Ref. [26] for complete details of the setup), where we image the fluorescence intensity at time intervals of 600 ms over a total duration of 15 min. Since at these concentrations the fluorescence intensity is proportional to concentration, it provides an indication for the concentration of the negative ion.

Figures 4(a)–4(c) present the fluorescence intensity around a single porous particle at different times in the

charging process. At short times ( $t = 6 \text{ s}$ ), a thin depletion region is formed around the disk. Notably, depletion is more significant around the poles of the disk, as predicted by the short-times analysis. At later times ( $t = 48 \text{ s}$ ), the asymmetry in the size of the depletion regions is clearly visible, as expected from the difference in mobility between sodium and fluorescein, and as predicted by the numerical simulation. We note that another source of asymmetry is the electro-osmotic flow on the chamber’s walls, which is directed along the electric field lines and acts to extend the depletion region around the negative pole. After 108 s, the depletion region is on the scale of the disk, and after another  $\sim 10 \text{ min}$ , the ionic flux from the surrounding bulk is balanced with the charging rate of the micropores, which leads to a quasisteady regime characterized by nearly static depletion regions (see Ref. [26] for data set). Consistent with our estimations for  $\tau_D$ , we indeed observe in our experiments (with no advection) charging times of tens of minutes and much more significant changes in concentration ( $\sim 1/3$ ) over larger distances ( $\sim a$ ) as compared to impermeable particles. In the Supplemental Material [26] we present a similar time-lapse experiment performed on a staggered array of disks (Fig. S6), and the discharge of fluorescein when the electric field is flipped (Fig. S8). In the presence of advection [Fig. 4(d), flow velocity  $600 \mu\text{m/s}$ ], the charging time reduces to approximately 15 min, as indicated by gradual disappearance of the the downstream depletion wake.

*Summary, conclusions, and future directions.*—We studied the electrokinetic response of a conducting porous particle to an externally applied electric field. As demonstrated by both our experimental and numerical results, the ICCDI phenomenon is characterized by charging time which is several orders of magnitude larger than that of a polarizable impermeable particle, and leads to significant

changes in salt concentration in the electrically neutral bulk. Consequently, in ICCDI the processes of electro-sorption, electromigration, diffusion, and advection are strongly coupled as they operate on similar time scales.

Several nonlinear effects are triggered by the strong electro-sorption of the porous particle, which merit further investigation. In the advection-free case, we observed sharp concentration fronts propagating away from the particle which are likely associated with conductivity and  $pH$  gradients induced by the particle. The formation of these gradients is particularly interesting, as those affect the electrophoretic mobility of the participating ionic species and thus couple back to electromigration and electro-sorption fluxes. Modeling of such multicoupled processes requires construction of more elaborate numerical schemes.

The effects we observed in this work may be particularly important when considering the electrophoretic mobility of such particles. Most importantly, the self-generated salt concentration gradient around the particle is expected to result in significant diffusiophoretic forces, which, depending on the species' diffusivities and the  $\zeta$  potential of the surface, may either retard or advance the particle. Furthermore, the above-mentioned  $pH$  changes may also have a significant influence on the native  $\zeta$  potential of the surface and also affect its mobility.

From a practical perspective, ICCDI may be useful for the implementation of novel desalination methods, as it allows rapid removal of ionic species without requiring physical connection of the electrode.

S. R. is supported in part by a Technion fellowship from the Lady Davis Foundation. We gratefully acknowledge the assistance of Mr. Eric Guyes in building the fluidic cell and thank Professor Martin Bazant for useful comments.

---

\*mberco@technion.ac.il

- [1] F. Reuss, Mem. Soc. Imp. Nat. Moscou **2**, 327 (1809).
- [2] H. V. Helmholtz, Ann. Phys. (Berlin) **243**, 337 (1879).
- [3] M. Z. Bazant and T. M. Squires, Phys. Rev. Lett. **92**, 066101 (2004).
- [4] O. Schnitzer and E. Yariv, Phys. Rev. E **86**, 061506 (2012).
- [5] S. M. Davidson, M. B. Andersen, and A. Mani, Phys. Rev. Lett. **112**, 128302 (2014).
- [6] C. Peng, I. Lazo, S. V. Shiyankovskii, and O. D. Lavrentovich, Phys. Rev. E **90**, 051002 (2014).
- [7] A. Johnson and J. Newman, J. Electrochem. Soc. **118**, 510 (1971).
- [8] R. De Levie, Electrochim. Acta **8**, 751 (1963).
- [9] J. S. Newman and C. W. Tobias, J. Electrochem. Soc. **109**, 1183 (1962).
- [10] J. Newman and W. Tiedemann, AIChE J. **21**, 25 (1975).
- [11] M. E. Suss, S. Porada, X. Sun, P. M. Biesheuvel, J. Yoon, and V. Presser, Energy Environ. Sci. **8**, 2296 (2015).
- [12] D. Dunn and J. Newman, J. Electrochem. Soc. **147**, 820 (2000).
- [13] R. Kötz and M. Carlen, Electrochim. Acta **45**, 2483 (2000).
- [14] P. Simon and Y. Gogotsi, Nat. Mater **7**, 845 (2008).
- [15] D. Brogioli, Phys. Rev. Lett. **103**, 058501 (2009).
- [16] R. A. Rica, R. Ziano, D. Salerno, F. Mantegazza, and D. Brogioli, Phys. Rev. Lett. **109**, 156103 (2012).
- [17] J. J. Bikerman, Trans. Faraday Soc. **35**, 154 (1940).
- [18] S. S. Dukhin, Adv. Colloid Interface Sci. **44**, 1 (1993).
- [19] F. C. Leinweber, J. C. Eijkel, J. G. Bomer, and A. van den Berg, Anal. Chem. **78**, 1425 (2006).
- [20] P. M. Biesheuvel, Y. Fu, and M. Z. Bazant, Russ. J. Electrochem. **48**, 580 (2012).
- [21] M. Eikerling, A. Kornyshev, and E. Lust, J. Electrochem. Soc. **152**, E24 (2005).
- [22] M. E. Suss, P. M. Biesheuvel, T. F. Baumann, M. Stadermann, and J. G. Santiago, Environ. Sci. Technol. **48**, 2008 (2014).
- [23] A. Hemmatifar, M. Stadermann, and J. G. Santiago, J. Phys. Chem. C **119**, 24681 (2015).
- [24] P. M. Biesheuvel, H. V. M. Hamelers, and M. E. Suss, Colloids Interface Sci. Commun. **9**, 1 (2015).
- [25] Z.-H. Huang, M. Wang, L. Wang, and F. Kang, Langmuir **28**, 5079 (2012).
- [26] See Supplemental Material at <http://link.aps.org/supplemental/10.1103/PhysRevLett.117.234502> for additional details, which include references [27,28].
- [27] R. J. Hunter, Foundations of Colloid Science (Oxford University Press, New York, 2001).
- [28] M. Mirzadeh, F. Gibou, and T. M. Squires, Phys. Rev. Lett. **113**, 097701 (2014).
- [29] K. T. Chu and M. Z. Bazant, Phys. Rev. E **74**, 011501 (2006).
- [30] COMSOL Multiphysics v. 5.1b, [www.comsol.com](http://www.comsol.com).
- [31] A. Zangwill, Modern Electrodynamics (Cambridge University Press, Cambridge, 2013).
- [32] M. Z. Bazant, K. Thornton, and A. Ajdari, Phys. Rev. E **70**, 021506 (2004).
- [33] D. Prieve, J. L. Anderson, J. P. Ebel, and M. E. Lowell, J. Fluid Mech. **148**, 247 (1984).
- [34] S. S. Dukhin and B. V. Deryaguin, Electrophoresis (Nauka, Moscow, 1976).
- [35] J. L. Anderson, Annu. Rev. Fluid Mech. **21**, 61 (1989).